Electrohydrodynamics of an ionic liquid meniscus during evaporation of ions in a regime of high electric field

Chase S. Coffman,* Manuel Martínez-Sánchez, and Paulo C. Lozano
Department of Aeronautics and Astronautics, Massachusetts Institute of Technology, Cambridge, Massachusetts 02139, USA

(Received 22 October 2018; revised manuscript received 21 February 2019; published 26 June 2019)

Numerical investigations are presented for an ionic liquid meniscus undergoing evaporation of ions in a regime of high electric field. A detailed model is developed to simulate the behavior of a stationary meniscus attached to a liquid feed system. The latter serves as a proxy for commonly utilized electrospray emitters such as needles and capillary tubes. Two solution families are identified for prototype liquid analogous to the ionic liquid 1-ethyl-3-methylimidazolium tetrafluoroborate (EMI-BF4). The first belongs to a regime of low electric field in which the meniscus is blunt and does not emit charge. The second belongs to a regime of high electric field in which a conelike meniscus produces charge from a sharp tip. Electrohydrodynamic features of the meniscus in this regime are presented. These reveal that the meniscus is Stokesian and hydrostatic and governed by conduction. The applied electric field influences both the shape of the meniscus and the current that it produces while the impedance of the feed system—which must be above a threshold value in order to ensure that the current, and therefore the flow, remains below a maximum value—influences the meniscus current but not the macroscopic shape. In general, this shape deviates from Taylor's idealized cone.

DOI: 10.1103/PhysRevE.99.063108

I. INTRODUCTION

Molecular and atomic ions are extractable from the surface of an electrified liquid through the agency of a strong electric field. This phenomenon serves as the foundation for the liquid metal ion sources (LMIS) that have found use in a variety of applications ranging from electric micropropulsion [1,2], etching and deposition [3], and analytical instrumentation [4]. Such broad technological utility has led to high levels of both empirical [5] and theoretically [6] development. Due to the high electrical conductivity, LMIS beams are generally typified by low energy spread and high current. The latter in particular is understood to be an integral component of the source in that it confers strong space charge effects that damp perturbations to the meniscus and provide a mechanism for stability [7]. Ionic liquids (ILs) are room temperature molten salts with conductivities that are small in relation to those of liquid metals. Emission of ions from such liquids is a more recent development with heritage in electrospray [8,9] but of significant interest on account of the wide spectrum of complex molecular chemistries to which they facilitate access. These include heavy ions that are useful in electric propulsion, where the thrust-to-power ratio scales as the root of the ion mass [10–12], and highly reactive ions capable of precision etching [13]. Unlike LMIS, ionic liquid ion sources (ILIS) emit more modest currents that typically preclude substantial space charge effects [14], giving the source a unique character that remains to be fully appreciated. Although ILIS are already finding application, improved understanding of their behavior is expected to serve as an important bridge to more robust service and expansion of use.

In the simplest electrospray configuration a liquid meniscus is formed at the end of a long tube or needle which is disposed in a dielectric medium. This could be vacuum [15], air [16], or an insulating liquid of sufficient dielectric strength [17]. The meniscus is stressed with an electric field that is applied through a relative bias between the tube or needle and a distant electrode. A well-established instability exists in the case of an electric field acting on the interface of two fluids. When the traction of the field is strong enough to overcome the binding effects of surface tension, a rapid rearrangement occurs in which the surface adopts a quasiconic geometry that serves to mediate a compromise between electrical and interfacial forces. The canonical structure, known commonly as a Taylor cone [15], supports a field that scales as $r^{-1/2}$, where r is the distance from the meniscus tip. In order to avoid a singularity at the tip, a thin jetlike protuberance will emanate from the zenith of this cone and usher charge under the action of electrical surface shear. The jet ultimately breaks into a fine, monodisperse aerosol as a result of capillary instability. The jet width, electrosprayed droplet size, and the droplet mass per unit charge are all proportional to the resistivity of the liquid and its flow rate through the cone [18,19]. External control of the flow rate and liquid conductivity are therefore useful tools in the regulation of the aerosol properties. In this way jets as small as 10 nm can be produced before the electric field acting on the surface of the cone-to-jet transition region becomes substantial enough to extract individual ions (no solvation) through a kinetic process akin to thermal evaporation [20,21]. This produces a mixed beam of droplets and ions that is characterized by a bimodal distribution of specific charge. The droplets provide a low specific charge peak while the ions

*Corresponding author: ccoffman@mit.edu

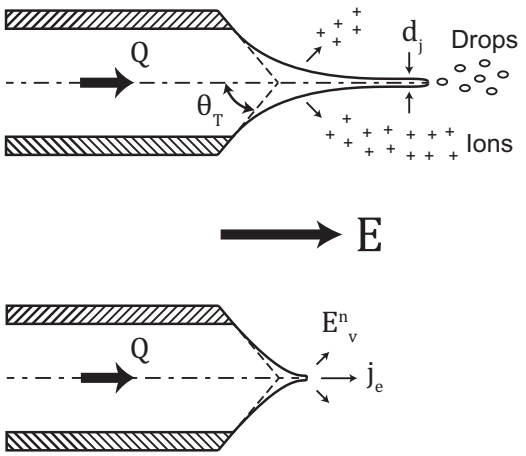

FIG. 1. Evolution of a cone-jet as the flow rate is reduced. Top: At high flow rates Q the meniscus resembles a classical Taylor cone (angle $\theta_T \approx 49.2^\circ$) and exhibits a characteristic protuberance at the tip. The tip supplies a train of electrosprayed droplets that propagate under the influence of the external field E. It may eventually shed ions and other charges of low solvation as its diameter d_j decreases in response to waning flow. Bottom: Under certain conditions, very low flow rates lead to complete extinction of the jet, such that only ions emanate from a sharp tip through electrically induced evaporation.

provide a much higher counterpart. Under certain conditions, further reductions to the flow facilitate complete extinction of the jet, such that ions evaporate in the absence of any droplets (Fig. 1). Aside from liquid metals [3], concentrated aqueous acids [22], and ILs [23,24] are among a very limited number of liquids known to support this unique mode of electrohydrodynamic charge emission.

The seminal work of Perel *et al.* in the late 1960s established, for the first time, the viability of the pure ion mode with nonmetallic liquids [22]. This work leveraged concentrated solutions of sulfuric acid but received little follow-up until the early 2000s when Romero-Sanz and colleagues extended the finding to ILs [23]. Recent work has shown that, in contrast to the amenability of the LMIS to a wide variety of emitter configurations, the ILIS is most compatible with a simple needle geometry. This owes primarily to the strong proclivity of tubes to sporadically generate droplets when the liquid does not satisfy an obscure combination of high conductivity and surface tension [25]. Currents vary roughly linearly with the applied electric field but typically reside in a range from approximately 100 nA to 1000 nA that is low in comparison to the output of common LMIS [26–28]. This limits space charge effects and apparently makes the quality of the source susceptible to the specific properties of the working liquid and the details of its emitter [14].

A clear understanding of the source and its relationship to key operating parameters has remained elusive as a result of several important empirical limitations. These include, e.g., the difficulty in resolving the morphology of the meniscus tip and its internal flow. Similarly to what has been done with cone-jets [29], where inferences based on the electrosprayed beam are insufficient for resolving key properties of the meniscus, several attempts have been made to approach this problem from a computational perspective. Collins explored incipient electrohydrodynamic tip streaming from leaky dielectric films and found that, in the limit as the charge relaxation time becomes the smallest global timescale, the tip begins to exhibit a conic cusp which is likely prerequisite to ion emission [30]. Higuera investigated a small (nanoscopic) sessile drop of ionic liquid undergoing steady evaporation [31]. A hydrostatic condition and conduction-limited charge transport were found to prevail. This paper builds on those works by advancing a basic ILIS continuum model that is germane to a meniscus of practical (microscopic) size serviced by a feeding architecture, where the latter is intended to capture important effects relating to the emitter. It is benchmarked against previous studies and used to study a family of ionic liquid emission solutions, recently reported by Coffman [32,33], that are believed to hold practical significance. Special emphasis is placed on generic features of the meniscus during emission and the influence of various parameters that are amenable to external control, such as the applied electric field, the meniscus size, and the impedance of the needle or feeding tube.

II. GOVERNING PHYSICS

A. Emission field, tip sharpness, and characteristic current

Evaporation of charged species from the surface of an electrified liquid meniscus formed *in vacuo* is a kinetic process taken to obey [34,35]

$$j_e = \sigma \frac{k_B T}{h} \exp\left[-\frac{\Delta G - G\left(E_n^v\right)}{k_B T}\right], \tag{1}$$

where j_e is the current emitted per unit surface area, σ is the local density of surface charge, k_B is Boltzmann's constant, T is the liquid temperature, h is Planck's constant, ΔG is an evaporation energy barrier for solvated species, and E_n^v is the normal component of the local vacuum electric field. $G(E_n^v)$ is a reduction factor due to E_n^v that assumes the form $G(E_n^v) = (q^3 E_n^v/4\pi\epsilon_0)^{1/2}$ for polar media based on the Schottky hump. Here q is the charge state of evolving species and ϵ_0 is the permittivity of vacuum. Since $\Delta G/k_B T$ is typically large in practical situations, little to no emission is seen until $\Delta G - G(E_n^v) = O(k_B T) \ll \Delta G$, such as when

$$E_n^v \approx \frac{4\pi\epsilon_0(\Delta G)^2}{q^3} \equiv E^*, \tag{2}$$

which is interpreted as a critical field for strong evaporation. Unlike hard-body or solid field emitters, e.g., hot cathodes, steady emission from the electrified meniscus is only permissible when the liquid interface is able to reach a mechanical balance between the forces of electrical traction and surface tension. To a good approximation it is therefore appropriate to take $\tau_n^e \sim 2\gamma/r^*$ near the tip, where τ_n^e is the normal electric traction in vacuum and r^* is the inverse of the characteristic tip curvature. After invoking the Maxwell tensor the former is expanded to yield $\tau_n^e = \epsilon_0/2[(E_n^v)^2 - \epsilon(E_n^l)^2 + (\epsilon - 1)E_t^2]$, where E_n^v and E_n^l are both orthogonal to the interface—on the vacuum and liquid sides, respectively—and consistent with the boundary relation for idealized surface charge, i.e., $\sigma = \epsilon_0(E_n^v - \epsilon E_n^l)$. E_t is the tangential electric field at the surface. The characteristic field within the

meniscus during emission will in general depend on the evaporation state and properties of the liquid but may be of order E^*/ϵ at most. Taking $E_n^l = \mathcal{O}(E^*/\epsilon)$ during evaporation with $E_t = 0$ at the tip by symmetry and $E_n^v \approx E^*$ yields $\epsilon_0(E^*)^2(\epsilon-1)/2\epsilon \sim 2\gamma/r^*$. Consistency with the use of the kinetic law, Eq. (1), requires $\epsilon \gg 1$, a condition which is effectively satisfied by many ionic liquids [36]. In the polar limit, the appropriate length scale for the meniscus tip is therefore

$$r^* = \frac{4\gamma}{\epsilon_0(E^*)^2} = \frac{q^6\gamma}{4\pi^2\epsilon_0^3(\Delta G)^4}. \tag{3}$$

The distance r^* here may be interpreted as the extent of the meniscus over which fields of order E^* act. As a result, the size of the area from which charge will emanate is $\pi(r^*)^2$ to first a approximation. The prevailing current is then of order $I^* \sim \pi(r^*)^2 j^*$, where j^* is a characteristic current density. This is determined by recognizing that charge transport in the liquid obeys $j = K_0 E_n^l$ when Ohm's law is valid and conduction dominates—see below for congruent findings. In the steady state, the motion of this charge must identically balance kinetic losses at the interface. Invoking Eq. (1) and imposing this condition with $E_n^v = E^*$ yields $j^* = K_0 E^* \epsilon^{-1}(1+\chi)^{-1}$. Note that the exponent from the general kinetic law vanishes now by virtue of the vacuum field E^*, which by definition requires the argument to be precisely zero. The factor in the denominator $\chi = hK_0/\epsilon\epsilon_0 k_B T$ is an important dimensionless group representing the ratio of the kinetic emission time $h/k_B T$ to the characteristic charge relaxation time $\epsilon\epsilon_0/K_0$ in the liquid. There are two asymptotic limits: In the liquid metal limit $\chi \gg 1$ as a result of very high electrical conductivity while the ionic liquid limit implies $\chi \ll 1$. The current density is then

$$j^* \approx \begin{cases} \frac{\epsilon_0 E^* k_B T}{h}, & \chi \gg 1 \\ \frac{K_0 E^*}{\epsilon}\left(1 - \frac{hK_0}{\epsilon\epsilon_0 k_B T}\right), & \chi \ll 1 \end{cases}. \tag{4}$$

The primary interest pertains to the latter case, where it is now clear that fields of the order E^*/ϵ do in fact prevail within the meniscus during strong evaporation. This is a direct result of limited conductivity. In the ionic liquid limit it follows that the characteristic current density must be of order $j^* \sim K_0 E^*/\epsilon$, and so for the total current

$$I^* = \frac{\pi(r^*)^2 K_0 E^*}{\epsilon} = \frac{K_0\gamma^2 q^9}{4\pi^2\epsilon\epsilon_0^5(\Delta G)^6}, \tag{5}$$

which is apparently very sensitive to the solvation barrier of evolving species. Typical ionic liquid properties include the solvation energy $\Delta G \sim 1$–2 eV [20,34], the ambient conductivity $K_0 \sim 1$ S/m [37], the dielectric constant $\epsilon \sim 10$–100 [36], the surface tension $\gamma \sim 0.01$–0.1 N/m [38], the specific charge $q/m \sim 10^6$ C/kg, the density $\rho \sim 10^3$ kg/m^3 [39], the nominal (room temperature) viscosity $\mu_0 \sim 0.01$–0.1 Pa-s [38,39], the thermal conductivity $k_T \sim 0.1$ W/m K [39], and the thermal capacity $c_p \sim 10^3$ J/kg K [39]. Under these conditions the characteristic electric field, tip size, and current are $E^* \sim 10^8$–10^9 V/m, $r^* \sim 10^{-8}$–10^{-7} m, and $I^* \sim 10^{-8}$–10^{-6} A, where the latter is a good indication of the spectrum of experimentally observed values [14]. Clearly, the very strong electric fields that are required to overcome the kinetic barrier presuppose a sharp meniscus tip.

B. Space charge

The high currents of liquid metals result in a cloud of ions surrounding the meniscus tip. The effects of this cloud on the local potential field are known to significantly influence the behavior of the source, in part by tempering the emission [7]. The more modest currents of ionic liquids accompany a rarefied form of this cloud [14]. Consider from the Poisson equation $\nabla \cdot \boldsymbol{E} = \rho_{sc}/\epsilon_0$ that the electric field induced by the ion cloud is $E_{sc}^* = \rho_{sc}^* r^*/\epsilon_0$. The space charge density $\rho_{sc}^* = j^*/v_{sc}^*$ depends on the evaporation current $j^* = K_0 E^*/\epsilon$ and a characteristic ion speed $v_{sc}^* = (2q\Phi_{sc}^*/m)^{1/2}$ that is determined through an interplay of kinetic and electric potential energies, i.e., $m(v_{sc}^*)^2 = q\Phi_{sc}^*$. The potential change near the tip is $\Phi_{sc}^* = E^* r^*$ and thus $E_{sc}^* = K_0/\epsilon\epsilon_0(mE^* r^*/2q)^{1/2}$. In relation to the characteristic evaporation field E^*,

$$\frac{E_{sc}^*}{E^*} = \frac{K_0}{\epsilon\epsilon_0}\left(\frac{r^*}{2E^*}\frac{m}{q}\right)^{1/2}, \tag{6}$$

where the right-hand side is the ratio of the gas-phase ion residence time, r^*/v_{sc}^*, to the charge relaxation time, $\epsilon\epsilon_0/K_0$. Under typical ionic liquid conditions this is small, from 10^{-2} to 10^{-1}, indicating that space charge effects are tenuous. Notice, however, that for liquid metals that the same analysis confirms the preponderance of space charge effects since $E_{sc}^*/E^* \to \infty$ in the perfect conductor limit.

C. Hydraulics

The flow of liquid induced by evaporation exhibits a characteristic velocity $u^* = j^*/\rho(q/m)$ near the meniscus tip. Due primarily to the high specific charge of ions, the corresponding Reynolds number $\mathrm{Re} = \rho u^* r^*/\mu_0$ and the ratio of viscous stresses to surface tension stresses-capillary number $\mathrm{Ca} = \mu_0 u^*/\gamma$—are both small, indicating a regime of Stokesian motion in a quasihydrostatic meniscus.

D. Transport processes

The balance of electrical surface shear, of order $\sigma E^*/\epsilon$, and viscous stress at the tip produces a flow of characteristic speed $u_\tau^* = \epsilon_0 E^{*2} r^*/\mu_0\epsilon$ that is comparable to u^*, i.e., $u_\tau^* = \mathcal{O}(u^*)$. The characteristic residence time for species moving through the meniscus tip is therefore r^*/u^*. The timescales for electrical and thermal conduction are, respectively, $\epsilon\epsilon_0/K_0$ and $\rho c_p(r^*)^2/k_T$. These are fast on the scale of the residence time, between 10 and 10^4 times shorter, indicating that convection processes are subordinate to conduction.

III. MODEL FORMULATION

Figure 2 depicts a meniscus model in which a volume of liquid is attached to a flat horizontal plate under vacuo with a prescribed wetting radius r_0 that could in general be much larger than r^*, as is typical in practice [14,23,25]. The plate comprises a hole of the same radius, r_0, causing the liquid contact line to remain pinned when the wetting angle is sufficiently high. For numerical convenience the plate is

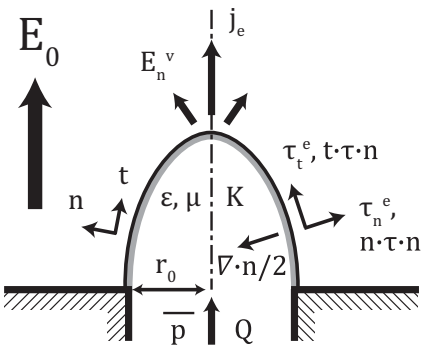

FIG. 2. Modeling configuration for an evaporating ionic liquid meniscus. An axisymmetric meniscus is attached to a conductive plate under vacuo with a contact radius r_0 (arbitrary contact angle) and stressed by an applied electric field E_0 that is asymptotically uniform at distances much greater than r_0 from the plate. Fresh liquid enters the meniscus during steady evaporation at a pressure $\overline{p}$ by a reservoir that is charged to a prescribed pressure p_r and a feeding line with characteristic impedance R_h.

infinite in the radial direction and assumed to be a perfect conductor. In connection with a distant counterelectrode this defines an axial electric field E_0 that is asymptotically uniform very far from the meniscus. The shape of the meniscus is contingent on a mechanical balance that is influenced in part by this field. A reservoir of liquid exists beneath the plate where it is charged to a pressure p_r and in communication through a feed line of characteristic impedance R_h, such that $p_r - \overline{p} = R_h Q$, where $\overline{p}$ is the mean pressure of the liquid on the plate and $Q = I(q/m)^{-1}/\rho$ is the flow rate due to evaporation.

The dimensionless equations and boundary conditions governing the problem of steady evaporation from this meniscus span two distinct domains (vacuum, liquid) and two boundaries (liquid-vacuum interface, plate). Lengths are scaled by the prescribed contact radius r_0, areas by r_0^2, stresses by the capillary pressure $p_c = 2\gamma/r_0$, electric fields by a value E_c satisfying $\epsilon_0 E_c^2 = p_c$ [11,40,41], charge densities by $\epsilon_0 E_c$, current densities by $K_0 E_c$, velocities by the corresponding speed $u_c = mK_0E_c/\rho q$, and temperatures by the reference value T_0. Conductivity and viscosity are scaled by the nominal values K_0 and μ_0, defined at ambient temperature. Scaling in this manner yields the dimensionless parameters

$$B = \frac{r^*}{r_0}, \quad \Lambda = \frac{K'T_0}{K_0}, \quad \psi = \frac{\Delta G}{k_B T_0}, \quad \chi = \frac{hK_0}{\epsilon\epsilon_0 k_B T_0},$$

$$\mathrm{We} = \frac{\rho(u^*)^2 r^*}{2\gamma}, \quad \mathrm{Ca} = \frac{\mu_0 u^*}{2\gamma}, \quad \mathrm{Gz} = \frac{\rho c_p u^* r^*}{k_T},$$

$$K_c = \frac{\epsilon\epsilon_0 u^*}{K_0 r^*}, \quad H = \frac{(j^* r^*)^2}{K_0 k_T T_0}, \quad C_R = \frac{K_0 E_c r_0^3}{2\gamma\rho}\left(\frac{m}{q}\right)R_H$$

as well as E_0, ϵ, and p_r. B is an important meniscus size parameter that will in general be much less than unity for conditions of interest. Λ is a parameter describing thermally induced perturbations to the electrical conductivity of the liquid, for which K' is an appropriate thermal sensitivity (S/m K), while ψ describes the emission kinetics. The constants We, Ca, and Gz are modified Weber, capillary, and Graetz numbers, respectively. K_c is the ratio of the charge relaxation time to the characteristic residence time of liquid in the meniscus tip. H is the ratio of Ohmic heat generation to conductive dissipation and C_R relates a characteristic pressure drop $K_0 E_c r_0^2 (m/q) R_H/\rho$ to surface tension.

A. Vacuum domain

Outside the liquid

$$\nabla^2 \phi^v = 0, \quad \text{with} \tag{7}$$

$$\boldsymbol{E}^v = -\nabla\phi^v, \tag{8}$$

where $-\nabla\phi^v \to E_0 \boldsymbol{i}$ very far from the meniscus, with $\boldsymbol{i}$ a unit vector normal to the plate.

B. Liquid domain

Inside the liquid

$$\nabla \cdot \boldsymbol{j} = 0, \tag{9}$$

$$\nabla \cdot \boldsymbol{v} = 0, \tag{10}$$

$$\epsilon^2 \mathrm{We}(\boldsymbol{v}\cdot\nabla)\boldsymbol{v} = \nabla\cdot\boldsymbol{\tau}, \tag{11}$$

$$\nabla^2 T + \epsilon^2 \frac{H}{B}\left(\frac{\boldsymbol{j}\cdot\boldsymbol{j}}{K}\right) - \epsilon\frac{\mathrm{Gz}}{\sqrt{B}}(\boldsymbol{v}\cdot\nabla T) = 0, \tag{12}$$

$$K = 1 + \Lambda(T-1), \quad \text{and} \tag{13}$$

$$\mu = K^{-1}, \tag{14}$$

where $\boldsymbol{j}$ and $\boldsymbol{v}$ are the current density and velocity in the liquid. Equations (9)–(11) represent charge continuity, mass continuity, and momentum conservation. In the latter, $\boldsymbol{\tau} = -p\boldsymbol{I} + \boldsymbol{\tau}'$ is a stress tensor with the viscous (deviatoric) component

$$\boldsymbol{\tau}' = \epsilon \mathrm{Ca}\sqrt{B}\mu[\nabla\boldsymbol{v} + (\nabla\boldsymbol{v})^T], \tag{15}$$

Equation (12) is a liquid heat equation with convection while Eqs. (13) and (14) describe the temperature-dependent electrical conductivity and viscosity. These assume a constant product $\mu K = \mu_0 K_0$ [42,43] and linear excursions of the form $K_0 + K'(T - T_0)$.

C. Liquid-vacuum interface

At the liquid-vacuum interface

$$\boldsymbol{\tau}_n^e - \boldsymbol{n}\cdot\boldsymbol{\tau}\cdot\boldsymbol{n} = \frac{1}{2}\nabla\cdot\boldsymbol{n}, \tag{16}$$

$$\boldsymbol{t}\cdot\boldsymbol{\tau}\cdot\boldsymbol{n} = \boldsymbol{\tau}_t^e, \tag{17}$$

$$\boldsymbol{v}\cdot\boldsymbol{n} = j_e \tag{18}$$

$$j_e = \frac{\sigma T}{\epsilon\chi}\exp\left(-\frac{\psi}{T}\left\{1 - B^{1/4}\sqrt{E_n^v}\right\}\right), \tag{19}$$

$$j_e - KE_n^l = K_c B^{3/2}\sigma(\boldsymbol{n}\cdot\nabla\boldsymbol{v}\cdot\boldsymbol{n}) - K_c B^{3/2}\boldsymbol{v}\cdot\nabla\sigma, \tag{20}$$

$$\sigma = E_n^v - \epsilon E_n^l, \tag{21}$$

$$I = \int j_e dA, \quad \text{and} \tag{22}$$

$$(\boldsymbol{n}\cdot\nabla)T = 0, \tag{23}$$

where $\boldsymbol{n}$ and $\boldsymbol{t}$ are unit vectors normal and tangent to the liquid surface, along which $\nabla\cdot\boldsymbol{n}$ is the local curvature. The superscripts v and l denote the vacuum and liquid sides, respectively. Equations (16) and (17) are balances of normal and tangential stresses involving the dimensionless Maxwell components [44,45]

$$\boldsymbol{\tau}_n^e = \left(E_n^v\right)^2 - \epsilon\left(E_n^l\right)^2 + (\epsilon-1)E_t^2, \tag{24}$$

$$\boldsymbol{\tau}_t^e = 2\sigma E_t, \tag{25}$$

where $E_n = \boldsymbol{E}\cdot\boldsymbol{n}$ and $E_t = \boldsymbol{E}\cdot\boldsymbol{t}$. Equations (18) and (19) are a kinematic condition and the kinetic evaporation rate. Equations (20)–(23) represent charge transport, surface charge density, total current, and thermal flux. Note that the charge transport equation is the central relationship governing the evolution of the surface charge. At the tip, this charge is especially critical for determining the character of the meniscus [30].

D. Plate

At the plate ($z = 0$)

$$\begin{aligned} &\boldsymbol{v} = \frac{I}{\pi}\boldsymbol{i}, \quad \overline{p} = p_r - IC_R \quad \text{for } r < 1,\\ &\Phi^l = 0, \quad T^l - 1 = 0 \quad \text{for } r < 1,\\ &\phi^v = 0, \quad T - 1 = 0 \quad \text{for } r > 1. \end{aligned} \tag{26}$$

Equations (26) assign reference values to the potential, temperature, and pressure of the liquid exiting the feeding line. Notice here that $\Phi^l = 0$ and $T^l/T_0 = 1$ are used to ensure that the liquid matches the ambient conditions of the plate. These should be good approximations insofar as the plate is a good electrical and thermal conductor. The flow emerging from the feeding line is assumed to be fully developed so that any pressure gradients in the radial direction are small.

IV. NUMERICAL METHOD

Stationary solutions satisfying the governing equations are computed using finite-element and iterative methods. An initial guess is made for the meniscus shape and parameterized in axisymmetric cylindrical space as $z = h(r)$, where h is some function of r defined on the dimensionless interval $r \in [0, 1]$. The meniscus corresponding to this shape is analyzed to determine the electrical, hydraulic, and thermal fields that would prevail if the surface were motionless, i.e., in a state of mechanical equilibrium. The vacuum region outside of the meniscus and the meniscus itself are included in these numerical calculations while the effects of the feeding architecture are expressed through the conditions of Eqs. (26) on the boundary of the numerical domain. The liquid flow upstream of the plate is treated analytically through a lumped impedance R_H that should in general be quantified by an independent analysis for specific feeding configurations. Partitioning of the model in this way has greatly enhanced the affordability of calculations.

The numerical fields are used to check the balance of normal stresses at the interface, Eqs. (16) and (17), and determine the status of the meniscus dynamics. The balance of tangential stress is always satisfied. If guess $z = h(r)$ does not coincide identically with an equilibrium shape, then a residue τ_n^r of the form

$$\boldsymbol{\tau}_n^e - \boldsymbol{n}\cdot\boldsymbol{\tau}\cdot\boldsymbol{n} - \tfrac{1}{2}\nabla\cdot\boldsymbol{n} = \tau_n^r \tag{27}$$

will in general exist on the surface. This residue relates in some way to the dynamics of the meniscus and implies a motion of the interface. Solutions for the stationary meniscus are, therefore, configurations in which $\tau_n^r \to 0$ globally. This is achieved here through a simple relaxation method permitting the interface to slowly evolve in the direction of its preferred equilibrium. Consider that for a prescribed $z = h(r)$ the corresponding surface tension (Laplace) pressure is given by $P_L = \nabla\cdot\boldsymbol{n}/2$. After expansion of the divergence term

$$h_{rr} + \frac{h_r}{r}\left(1 + h_r^2\right) - 2\left(1 + h_r^2\right)^{3/2}P_L = 0, \tag{28}$$

where h_r and h_{rr} are the first and second spatial derivatives of $z = h(r)$, respectively. This is a second order nonlinear ordinary differential equation that maps between $P_L(r)$ and a corresponding shape. Now consider an initial meniscus guess $z = h^i(r)$ for which the attendant residue $(\tau_n^r)^i$ is nonzero. In an effort to reduce the residue for a subsequent iteration the interface may be relaxed by adding to the current Laplace distribution P_L^i a small measure of $(\tau_n^r)^i$, such that

$$P_L^{i+1} = P_L^i + \beta\left(\tau_n^r\right)^i. \tag{29}$$

Here β is a relaxation parameter residing on the interval $\beta \in (0, 1]$ that helps to control the rate of interfacial evolution. An updated shape $z = h^{i+1}(r)$ is found after solving Eq. (28) with $P_L = P_L^{i+1}$ and used to initiate a new set of calculations for which it is generally expected that $(\tau_n^r)^{i+1} < (\tau_n^r)^i$. Provided a stationary meniscus exists for the given parameter set, after many relaxing iterations the residues become sufficiently small. Numerical termination is therefore invoked when the condition

$$\frac{\tau_n^r}{\tau_R} \leqslant \Theta \tag{30}$$

is satisfied. τ_R is a reference stress and Θ is a number much less than unity. In most cases that follow these numerical parameters are taken as $\Theta = 10^{-2}$, $\beta = 10^{-2}$, and $\tau_R = \|\tau\|_\infty$, where $\|\tau\|_\infty$ is the local maximum norm (largest local stress). Note that the max norm is typically $\boldsymbol{\tau}_n^e$, particularly in proximity to the meniscus tip, while Θ ensures that the residue is never greater than 1% of any dominant stress.

V. RESULTS AND DISCUSSION

Direct empirical validation of the model is challenging on account of the absence of high-resolution meniscus visualizations. The literature is, however, replete with theoretical investigations of electrified interfaces—see, e.g., Refs. [15,46,47]. Most cases treat sessile or pendant drops for which the volume

is invariant. Such situations can be addressed with the present model by substituting

$$\overline{p} = p(E_0, \mathcal{V}) \tag{31}$$

for the pressure relation $\overline{p} = p_r - IC_R$ describing the effects of the feeding flow. The constant-volume $\overline{p}$ may be identified iteratively as an extra step in the numerical method. This procedure is used here to benchmark the model against the findings of Higuera for ion emission from ionic liquid sessile drops [31]. Dielectric drops (no emission) are investigated elsewhere [33] and contrasted with the findings of Wohlhuter and Basaran [47].

The generalized (free-volume) meniscus problem with feeding flow is treated thereafter in the case of small B where the contact line r_0 is large in comparison to the characteristic tip size r^* since this is the situation that is most commonly encountered in practice [14,23,25]. A test liquid is designed with properties similar to those of 1-ethyl-3-methylimidazolium tetrafluoroborate (EMI-BF4), an IL that is widely employed in empirical evaporation studies [10,11,23]. The neat IL is modeled at room temperature ($T_0 = 300$ K) using $K_0 = 1$ S/m, $K' = 0.04$ S/m K, $q/m = 10^6$ C/kg, $\mu_0 = 0.037$ Pa s, $k_T = 0.2$ W/m K, $c_p = 1500$ J/kg K, $\gamma = 0.05$ N/m, $\Delta G = 1$ eV, and $\rho = 10^3$ kg/m^3. Note that the dielectric constant $\epsilon = 10$ is appropriate [36] but relatively apolar in comparison to those of typical electrolytic solutions, e.g., aqueous solutions. These properties establish the dimensionless parameters $\Lambda = 12$, $\psi = 38.6$, $\chi = 1.81 \times 10^{-3}$, $\mathrm{We} = 2.26 \times 10^{-6}$, $\mathrm{Ca} = 0.026$; $\mathrm{Gz} = 0.024$, $K_c = 1.32 \times 10^{-4}$, and $H = 0.176$, while those that remain (E_0, P_r, B, C_R) form a subspace that is explored numerically. Two primary solution families are identified: one spanning a regime of low electric field for which meaningful emission is absent and another in a regime of high electric field where evaporation is substantial. The former is established in the literature [46–49] while the latter has only recently been reported by Coffman [32,33]. The high-field family is expanded on here. A prototype solution is presented to highlight electric, hydraulic, and thermal properties of the meniscus which are representative of the regime. The meniscus is sized $B = 0.05$ in this case to preserve ease of graphical representation while still ensuring that it reasonably resides in the small-B limit. The dependence of the meniscus morphology and emission current on the applied field, meniscus size, and feeding flow setup are also delineated to emphasize important relationships to external variables. These are shown for the specific case $p_r = 0$, chosen for its numerical economy and relevance to practical configurations, e.g., solid needle electrospray emitters.

A. Constant-volume meniscus

Solution in the low-field regime are bracketed by the null field $E_0 = 0$ on one side and a nonzero electric field corresponding to a "turning point" on the other [46,47]. When the elongation of the meniscus is defined as $Z_e = z_0/r_0$, where $z_0 = h(r = 0)$ is the height of the meniscus on the axis of symmetry, the turning point coincides with the field at which the incremental elongation ceases to be bounded, i.e., $dZ_e/dE_0 \to \infty$. Two solution branches comprise this family: an unstable branch of sharp menisci (high elongation) and a stable counterpart typified by rounded structures [15]. Only the latter is physical. The menisci of perfectly conducting liquids [15], insulating liquids [47–49], and ionic liquids [33] are all qualitatively similar on this branch.

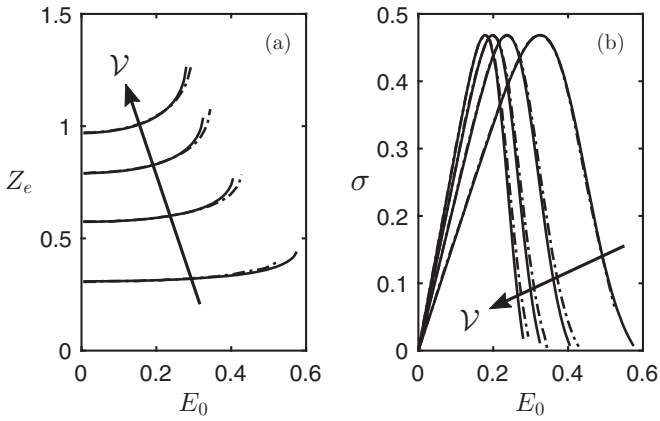

FIG. 3. Comparison of evaporation results for ionic liquid droplets of constant volume. The findings of Higuera [31] for volumes $\mathcal{V} = 0.5$, 1, 1.5, and 2 (dashed curves) are shown next to those computed with the present model. (a) Elongation of the droplets, $Z_e = h(r = 0)$, as a function of applied electric field. The droplet volume is increasing in the direction of increasing elongation. (b) Surface charge σ at the tip of the meniscus. The droplet volume increases from right to left.

Higuera [31] has modeled the shapes and evaporation properties of ionic liquid sessile droplets on the stable branch using time-resolved techniques. Axisymmetric droplets are attached to a conductive plate with constant wetting radius r_0 and volume $\mathcal{V}$. The liquid medium is relatively polar ($\epsilon = 50$) but permits evaporation of ions with very high specific charge when the applied electric field is sufficiently strong. Droplet volumes include $\mathcal{V} = 0.5$, 1, 1.5, and 2 with $B = 0.25$, where the latter implies meniscus sizes of order r^*. The liquid properties are $\epsilon = 50$, $\chi = 4.12 \times 10^{-4}$, $\psi = 20$, and $\mathrm{Ca} = K_c = \Lambda = \mathrm{We} = \mathrm{Gz} = H = 0$. Figure 3 presents a comparison of select results from the reference with those attained by the model described in this work. These are represented by dashed and solid curves, respectively. Figure 3(a) delineates the elongation Z_e of the meniscus in response to E_0, showing that the stationary meniscus extends weakly in response to low electric fields before terminating at a turning point. Figure 3(b) delineates the surface charge computed at the meniscus tip. Depletion of charge at the surface beyond a threshold field (decreasing σ) is indicative of emission and a symptom of the inability of electrical conduction (limited K) to keep pace with the rate of ion extraction at the interface.

The model confirms the results of the Higuera [31] and suggests that small menisci with B of order unity are capable of supporting emission for fields E_0 below that of the turning point. When B is small, however, they imply that emission is not likely to take place since the surface field is unable to reach sufficient strength. This can be appreciated by considering that, at the null field, the meniscus is subject to a simplified mechanical balance $\overline{p} = \nabla \cdot \boldsymbol{n}/2$ that produces a spherical section for which $r_0\kappa_t$ may be small depending on the size of the contact line and the drop volume. Here κ_t^{-1} is the radius of

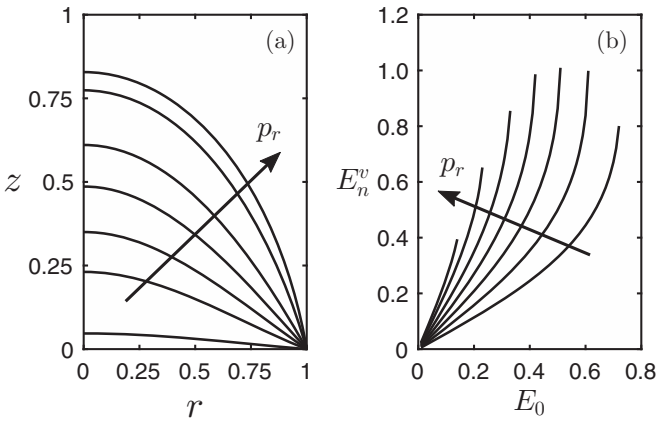

FIG. 4. Select characteristics of solutions in the low-field regime for $p_r = -0.50$, -0.25, 0, 0.25, 0.50, 0.75, and 0.90. (a) Limiting meniscus shapes at the end of the stable solution branch (turning point) in the low-field regime with electric field $E_0 = 0.72$, 0.61, 0.52, 0.42, 0.33, 0.23, and 0.14, respectively. The reservoir pressure increases in the direction of increasing elongation. (b) Electric field E_n^v at the tip of the meniscus. The maximum field corresponds to the turning point (maximum curvature) but remains limited to $E_n^v = \mathcal{O}(1)$, precluding emission from a large meniscus. The reservoir pressure decreases from left to right.

curvature of the meniscus tip. Although he meniscus elongates and sharpens as the field is increased, $r_0\kappa_t$ is at most of order unity as the turning point is reached. The electric field acting at the tip is therefore $E_n^v = \mathcal{O}(E_c)$. Since the scale E_c is related to the characteristic evaporation field E^* through the size parameter B, i.e., $E_c/E^* = B^{1/2}$, this indicates that the ratio $E_n^v/E^* \sim B^{1/2}$ is of a low magnitude when the meniscus is large, precluding meaningful emission. Coupled with the fact that the turning point typically coincides with the highest field for which stationary solutions, this provides strong evidence to suggest that the low-field regime does not correspond to the emission observed in practice [47].

B. Meniscus with feeding flow

Solutions to the generalized problem with a feeding architecture ($\overline{p} = p_r - IC_R$) in the low-field regime are qualitatively similar to those of the constant-volume drop. Figure 4(a) depicts meniscus shapes at the turning point for various p_r. These exhibit the limiting (highest) tip curvature in this regime. Figure 4(b) depicts the corresponding tip field. Note that the electric field at the turning point is in general a function of the reservoir pressure, decreasing in the direction of increasing p_r. This is similar to the sessile droplet case in which the turning point field decreases in inverse proportion to the droplet volume—see Fig. 3(a). Due to the lack of emission when $B \ll 1$, these results are independent of the feeding impedance C_R.

Stationary solutions of the low-field regime cease to exist as the electric field is increased infinitesimally at the turning point. This is generically true in the large meniscus limit, the properties of the liquid notwithstanding. A second family of solutions may, however, exist in a region of high electric field under special conditions [32,33]. The extent of this region is finite and does not overlap that of the low-field regime. Unlike the blunt "egglike" structures that typify the low-field regime, the meniscus in this regime is "conelike," supporting emission from a sharp tip.

Figure 5 presents salient properties of a high-field prototype solution calculated at $E_0 = 1.0$, $B = 1/20$, $C_R = 10^3$, and $p_r = 0$. Figure 5(a) depicts the shape of the meniscus while Figs. 5(b)–5(d) show the stress distribution, the electric potential, and the surface charge of the interface, respectively. Here, the potential is normalized by the characteristic loss through the tip $\Phi^* = E^* r^*/\epsilon$ and the surface charge by $\epsilon_0 E_n^v$, the value corresponding to the condition of full electrical relaxation. Figures 5(e) and 5(f) depict components of the flow field at the interface and its temperature distribution. The temperature scale $\Delta T^* = K_0 \Phi^{*2}/k_T$ follows from a balance of Ohmic dissipation and thermal conduction.

Figure 5(a) reveals the conelike nature of the meniscus in this regime but highlights a substantial deviation from the Taylor archetype. The idealized Taylor cone is predicated on a simple mechanical interaction in which electrical traction and surface tension globally equilibrate along a surface that is of uniform potential [15]. The electric field E_n^v in this case varies generically as $r^{-1/2}$, where r is the cylindrical radius, admitting a discrete spectrum of spherical harmonics. Only the Legendre function $P_{1/2}$ is permitted on the surface. Due to the location of the corresponding zero, classical Taylor cones exhibit a universal 49° half-angle that is insensitive to the intrinsic properties of the liquid. Deviation from this cone represents a fundamental finding but should perhaps come as no surprise since the mechanical balance is evidently more complex. In addition to electrostatic traction and surface tension, hydraulic pressure is seen to play a meaningful role over much of the meniscus, particularly away from the tip [Fig. 5(b)]. This is so much so that the balance in this specific case essentially excludes surface tension near the base, resulting in a liquid surface that is almost coplanar with the plate.

Morphological deviations from Taylor notwithstanding, depletion of charge from the tip [Fig. 5(d)] and a corresponding potential drop [Fig. 5(c)] indicate that the meniscus is sharp enough under the given conditions to emit meaningful charge. The current is approximately 160 nA for the test liquid. In providing this charge the meniscus is found to be hydrostatic and conduction controlled. Notice that the tip is encircled by a curve $\mathcal{C}$ on which the electric field coincides with the characteristic value E^*. Since the field varies smoothly over the meniscus the exponent from the kinetic law, Eq. (1), is of very dissimilar magnitudes on either side of this line. Toward the tip its growth outpaces transport in the liquid and results in a reduction of the local surface charge from its equilibrium value $\epsilon_0 E_n^v$. The flow upstream of this region is primarily tangent to the interface but turns orthogonal (from the meniscus) on crossing the line $\mathcal{C}$. The maximum flow speed is of order u^* from Fig. 5(e), ensuring both the Stokesian hydrostatic character of the meniscus and the governance of conduction. The former is further evidenced by the stress distribution across the interface [Fig. 5(b)], which implies that the effects of flow through the meniscus are relatively insignificant and that the interplay of electrical traction and surface tension dominates at the tip. Away from

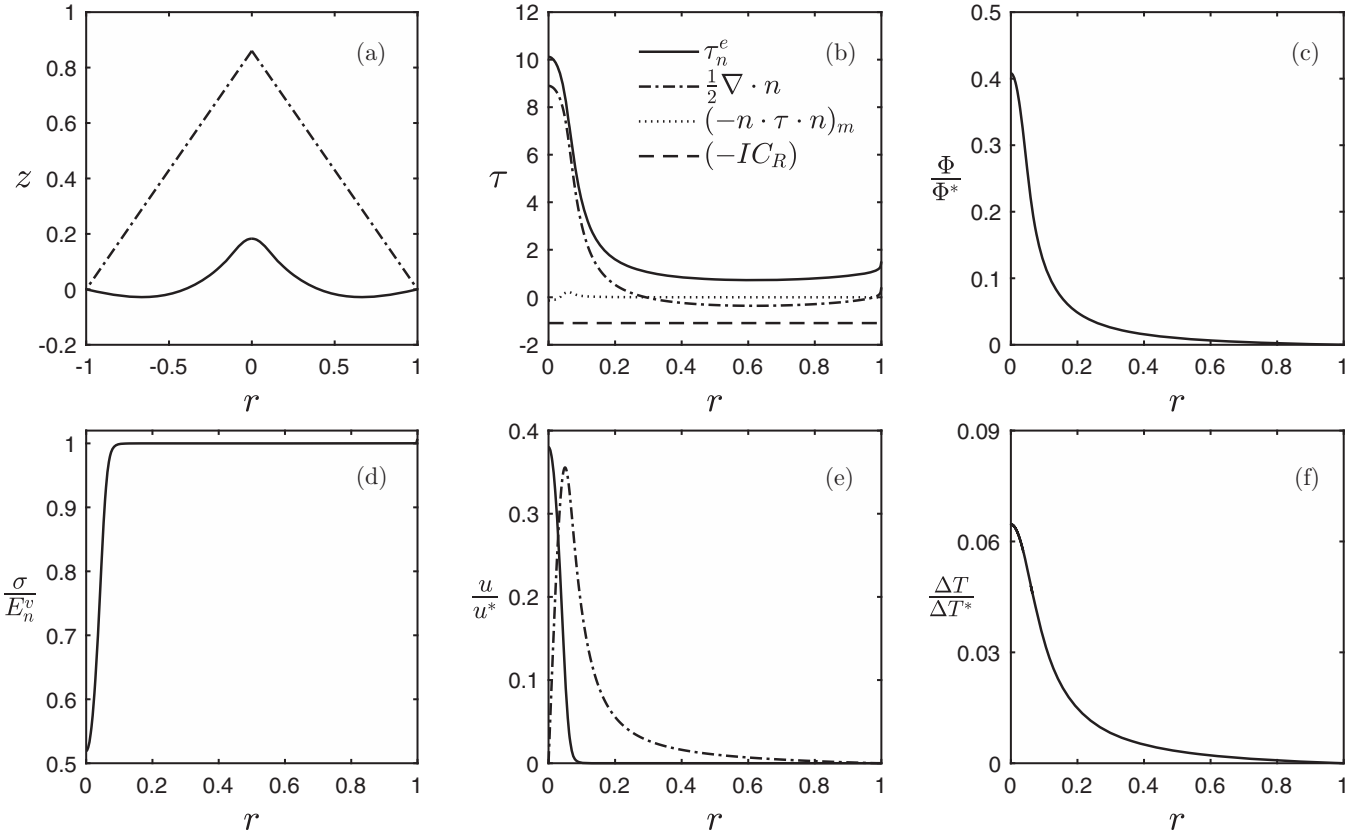

FIG. 5. Select properties of the steadily evaporating meniscus residing at the point $E_0 = 1$, $1/B = 20$, $P_r = 0$, and $C_R = 10^3$ in parameter space. (a) The meniscus shape (solid curve) plotted alongside a classical Taylor cone (dashed curve) for comparison. (b) The distribution of stresses across the liquid-vacuum interface. The viscous stress accumulated in the meniscus itself, $(-\boldsymbol{n} \cdot \boldsymbol{\tau} \cdot \boldsymbol{n})_m$, is separated from the pressure drop in the feeding line, $-IC_R$, for clarity. (c) The distribution of electric potential across the liquid-vacuum interface, normalized by the characteristic $\Phi^* = E^* r^*/\epsilon_r$. (d) The distribution of surface charge across the liquid-vacuum interface, normalized by the normal component of the displacement field in vacuum. (e) Normal (solid curve) and tangential (dashed curve) components of the fluid flow at the liquid-vacuum interface, normalized by the characteristic u^*. (f) The temperature of the liquid-vacuum interface normalized by ΔT^*.

the tip, only the pressure of the liquid on the plate $-IC_R$ is a factor.

The potential drop through the meniscus has important implications insofar as the energy of the emanating beam is concerned. Charge must be conducted through the tip region by a potential drop of order Φ^* [Fig. 5(c)] since the convected current $\epsilon_0 E^* u^*/r^*$ is nominal. The speed u^* is small in comparison to the velocity of an ion after electrostatic free-fall through the same potential, $(q\Phi^*/m)^{1/2}$, and so the resistivity of the liquid is seen to reduce the kinetic energy of emitted ions from the theoretical maximum by an amount—several volts for common ILs—that is discernible on the scale of typical driving voltages (0.1–1 kV). This could be one explanation for the energy deficits observed in ionic liquid ion sources [24,28].

Figure 6 delineates the dependence of the meniscus morphology and the current on the meniscus size, the applied electric field, and the feed impedance. Figure 6(a) depicts a sequence of meniscus shapes for $E_0 = 0.7$ and $C_R = 10^3$ as the size is increased from $B^{-1} = 3.19$ to 100. Note that the upper limit of this size range is a computational threshold beyond which calculations typically lose affordability on account of stiffness. While stationary solutions may exist for larger menisci, the findings of Coffman *et al.* [32] suggest that a limit of tenability may exist as $B \to 0$. The corresponding tip sharpness is presented in Fig. 6(d). Here the curvature of the meniscus at the tip is $\kappa_t = 1/r_t = (\boldsymbol{\nabla} \cdot \boldsymbol{n})_t/2$, and thus the relationship to the characteristic emission scale becomes $r_t/r^* = 2/B(\boldsymbol{\nabla} \cdot \boldsymbol{n})_t$. Figure 6(b) shows variations in the shape of the meniscus for $B^{-1} = 106$ and $C_R = 10^3$ as the field is varied from $E_0 = 0.585$ to $E_0 = 0.685$. Experience with the model suggests that these fields approximately represent the range of feasible E_0 for a meniscus of this size. Notice that the low end of this range is somewhat larger than the field corresponding to the turning point for the meniscus with $p_r = 0$, i.e., $E_0 \approx 0.52$, but not dramatically so. Figure 6(e) depicts the emitted current over the same range normalized by I^*, where $I^* = 477$ nA for the prototype liquid, while Fig. 6(c) shows the relationship between the normalized current I/I^* and the feed impedance with $E_0 = 0.62$ and $B^{-1} = 106$. Values of C_R used to generate this data span several orders of magnitude between $C_R = 3.3 \times 10^6$ (arbitrary cutoff) and a value $C_R = 670$ below which stationary solutions could not be computed. Figure 6(d) elucidates the dependence of the tip morphology on C_R.

These suggest that the meniscus shape regularizes as B becomes increasingly small and then varies only as a function of the applied electric field while emitting a current of order

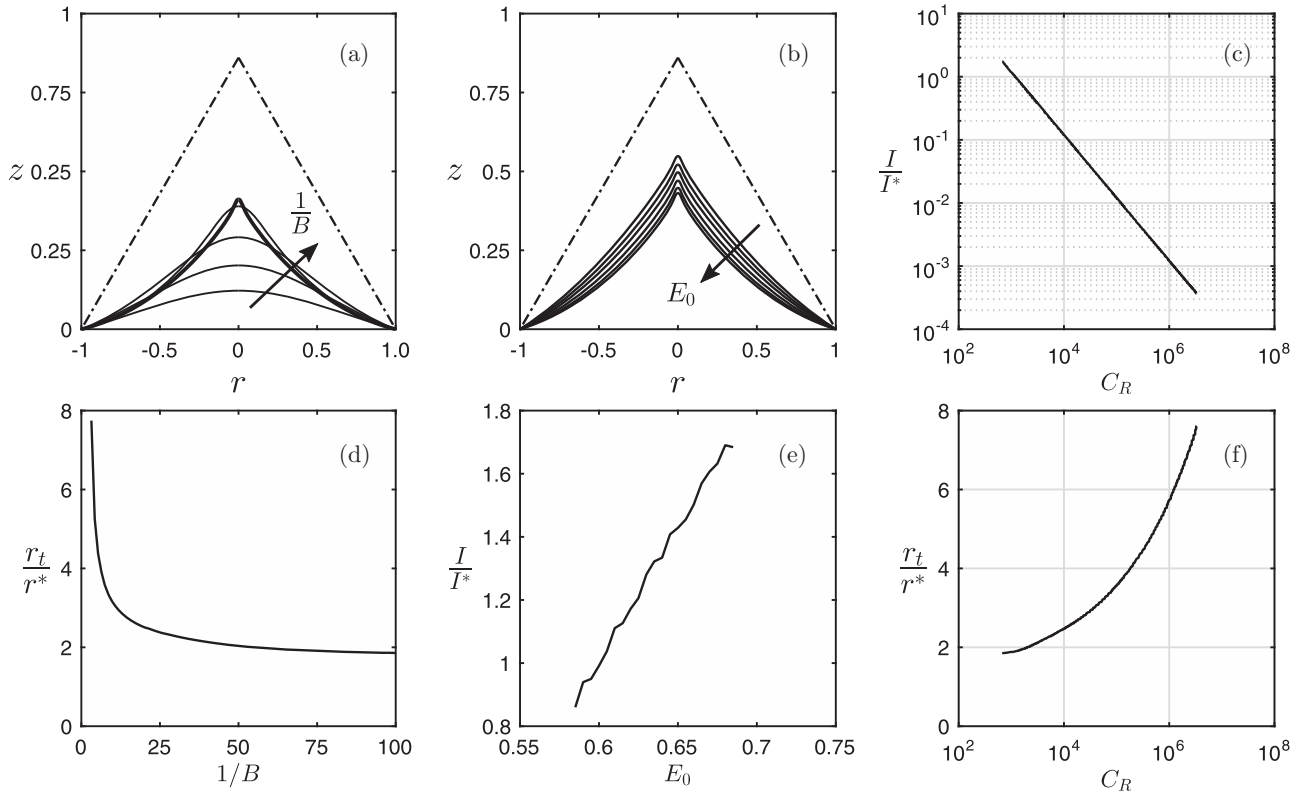

FIG. 6. Select parametric characteristics in the high-field regime. Effects of the meniscus size [(a) and (d)], electric field [(b) and (e)], and impedance [(c) and (f)] are represented. (a) Meniscus shapes for $E_0 = 0.7$ and $C_R = 10^3$. The meniscus size $1/B = 3.19, 4.26, 6.38, 17.0, 100$, increasing in the direction of increasing elongation. A classical Taylor cone (dashed) provides spatial reference. (b) Meniscus shapes for $1/B = 106$ and $C_R = 10^3$. The electric field $E_0 = 0.585, 0.605, 0.625, 0.645, 0.665, 0.685$, increasing in the direction of decreasing elongation. A classical Taylor cone (dashed) provides spatial reference. (c) Electrical current for $E_0 = 0.62$ and $1/B = 106$ over a range of impedance. (d) Radius of curvature at the meniscus tip for $E_0 = 0.7$ and $C_R = 10^3$ over a range of B. (e) Electrical current for $1/B = 106$ and $C_R = 10^3$ over a range of field. (f) Radius of curvature at the meniscus tip for $E_0 = 0.62$ and $1/B = 106$ over a range of impedance.

I^* that may be the maximum which the source is capable of supporting. The meniscus is initially blunt when $B = \mathcal{O}(1)$ but begins to adopt a conic profile as the size is progressively increased to the point at which the shapes are essentially indistinguishable on the macroscopic scale of the base for all $B \gtrsim 25$ [Fig. 6(a)]. This is accompanied by an asymptotic reduction of the tip to a radius of order r^* [Fig. 6(d)] and current of order I^*. Conduction ensures that subsequent changes to the field are met with linear variations of the latter [Fig. 6(e)], congruent with many empirical observations [10,11]. The pressure relationship $\overline{p} = p_r - IC_R$ requires that these result in a change to the liquid pressure on the plate. As the field and the current both increase, this is manifested as a decrease is in the elongation of the meniscus which makes it appear as though it is being slowly "sucked" back in the direction of the plane $z = 0$ [Fig. 6(b)]. Unlike the field, the feed impedance is found to influence the current of the source but not its macroscopic shape. Closer inspection reveals this interesting finding to be a byproduct of subtle changes to the microscopic morphology of the tip. The tip sharpens or dulls as needed to supply the necessary charge, and this apparently provide a mechanism for controlling the total current with minimal effect on the overall shape [Fig. 6(f)]. The macroscopic invariance implies that the pressure of the liquid emerging from the tube $\overline{p} = -IC_R$ is fixed over the range of C_R considered and it follows that the current must vary in inverse proportion to the impedance [Fig. 6(c)]. This is potentially a useful tool for regulating the brightness of the source. There may however be limits on the extent to which it is feasible since stationary solutions could not be computed as C_R approached a threshold value for which the current was not much larger than I^*. A possible explanation is that this is symptomatic of a tip which can be no smaller than r^*. Insofar as a droplet with $B \sim 1$ can be taken as a proxy for the tip of a much larger meniscus, the findings of Higuera strongly support this notion [31]. Given that the pressure of the liquid on the plate $\overline{p}$ is of order unity, if this is indeed the case it would imply that stationary solutions necessarily require $C_R = \mathcal{O}(\epsilon B^{-3/2})$ to ensure that the current remains within feasible limits, i.e., of order I^* or smaller.

VI. CONCLUSIONS

A mathematical model has been formulated to describe the behavior of an electrified ionic liquid meniscus undergoing evaporation of ions. The meniscus is attached to a liquid feed system that serves as a proxy for the needles and capillary tubes commonly used in electrospray practice. The amenability of the ionic liquid 1-ethyl-3-methylimidazolium tetrafluoroborate to pure ion evaporation is well established. The model is used to study the stationary properties of a prototype

liquid of similar character over a range of empirically relevant conditions. These include the size of the meniscus, the applied electric field, and the impedance of the feed system. Two distinct solution families are identified when the meniscus is large in comparison to a characteristic length scale for emission. The first belongs to a regime of low electric field and is typified by a relatively blunt "egglike" meniscus that does not emit charge. The second belongs to a regime of high electric field in which a sharp meniscus supports ion evaporation from its tip. This meniscus is "conelike" but still deviates substantially from a perfect 49.2° Taylor cone. In this regime the results indicate that the meniscus is hydrostatic and that only a small portion of the tip is active in the emission of charge. The surface of the meniscus is electrically shielded outside of the active region and depleted of interfacial charge within it, such that the local behavior is analogous to that of a dielectric. The effects of convection are tenuous and conduction dominates. Variations in electric current are therefore linear with respect to the applied field. Increases to the field increase the current and reduce the hydrostatic pressure of the meniscus, leading to a reduction of its elongation (height). Unlike the field, the feed impedance influences the current but does not control the macroscopic shape of the meniscus. Microscopic changes to the morphology of the tip are instead responsibly for regulating the outflow of charge. The sharpness of the tip and therefore the current are inversely related to the impedance in a way that ensures invariance of the liquid pressure, indicating that the meniscus shape is a function of only the applied electric field. The current can be increased by modulating the feed impedance only until it is of the maximum characteristic order, corresponding to the minimum characteristic tip size, at which point stationary solutions begin to lose tenability.

Future work should strive to incorporate dynamics in the model and investigate various instabilities to identify solutions that are physical. The effects of space charge, albeit tenuous, should also be investigated to better quantify their significance in relation to other important facets of the source. Empirical corroboration is also of critical importance and direct meniscus visualizations are expected to be indispensable in this regard. Efforts to obatain these will, however, necessitate very careful experimental planning and execution since μm-scale menisci and their sub-μm-scale features present inherent imaging challenges.

ACKNOWLEDGMENTS

The Air Force Office of Scientific Research and NASA Space Technology Research Fellowships program are acknowledged for financial support.

[1] M. Tajmar, A. Genovese, and W. Steiger, J. Propul. Power **20**, 211 (2004).
[2] M. Tajmar, I. Vasiljevich, and W. Grienauer, Ultramicroscopy **111**, 1 (2010).
[3] P. D. Prewett and G. L. R. Mair, *Focused Ion Beams from Liquid Metal Ion Sources* (Wiley, New York, 1991).
[4] G. L. R. Mair, Int. J. Mass Spectrom. Ion Process. **114**, 1 (1992).
[5] G. Benassayag, P. Sudraud, and B. Jouffrey, Ultramicroscopy **16**, 1 (1985).
[6] F. J. Higuera, Phys. Rev. E **69**, 066301 (2004).
[7] L. W. Swanson, Appl. Phys. A **41**, 223 (1986).
[8] J. F. de la Mora, Annu. Rev. Fluid Mech. **39**, 217 (2007).
[9] A. M. Gañán-Calvo, J. M. López-Herrera, M. A. Herrada, A. Ramos, and J. M. Montanero, J. Aerosol Sci. **125**, 32 (2018).
[10] J. R. S. Legge and P. C. Lozano, J. Propul. Power **27**, 485 (2011).
[11] D. G. Courtney, H. Q. Li, and P. Lozano, J. Phys. D **45**, 485203 (2012).
[12] G. Lenguito and A. Gomez, J. Microelectromech. Sys. **23**, 689 (2014).
[13] C. Perez-Martinez, S. Guilet, N. Gogneau, P. Jegou, J. Gierak, and P. Lozano, J. Vac. Sci. Technol. B **28**, L25 (2010).
[14] S. Castro and J. F. de la Mora, J. Appl. Phys. **105**, 034903 (2009).
[15] G. Taylor, Proc. R. Soc. A **280**, 383 (1964).
[16] J. Zeleny, Phys. Rev. **10**, 1 (1917).
[17] A. Barrero, J. M. López-Herrera, A. Boucard, I. G. Loscertales, and M. Márquez, J. Colloid Interface Sci. **272**, 104 (2004).
[18] J. F. de la Mora and I. G. Loscertales, J. Fluid Mech. **260**, 155 (1994).
[19] A. M. Gañán-Calvo, J. Dávila, and A. Barrero, J. Aerosol Sci. **28**, 249 (1997).
[20] M. Gamero-Castaño and J. F. de la Mora, J. Chem. Phys. **113**, 815 (2000).
[21] M. Gamero-Castaño, Phys. Rev. Lett. **89**, 147602 (2002).
[22] J. Perel, J. F. Mahoney, R. D. Moore, and A. Y. Yahiku, AIAA J. **7**, 507 (1969).
[23] I. Romero-Sanz, R. Bocanegra, J. F. de la Mora, and M. Gamero-Castaño, J. Appl. Phys. **94**, 3599 (2003).
[24] P. Lozano and M. Martínez-Sánchez, J. Colloid Interface Sci. **282**, 415 (2005).
[25] D. Garoz, C. Bueno, C. Larriba, S. Castro, I. Romero-Sanz, J. F. de la Mora, Y. Yoshida, and G. Saito, J. Appl. Phys. **102**, 064913 (2007).
[26] C. Larriba, S. Castro, J. F. de la Mora, and P. Lozano, J. Appl. Phys. **101**, 084303 (2007).
[27] S. Castro, C. Larriba, J. F. de la Mora, P. Lozano, S. Sumer, Y. Yoshida, and G. Saito, J. Appl. Phys. **102**, 094310 (2007).
[28] P. Lozano, J. Phys. D: Appl. Phys. **39**, 126 (2006).
[29] M. Gamero-Castaño and M. Magnani, J. Fluid Mech. **859**, 247 (2019).
[30] R. T. Collins, J. J. Jones, M. T. Harris, and O. A. Basaran, Nat. Phys. **4**, 149 (2008).
[31] F. J. Higuera, Phys. Rev. E **77**, 026308 (2008).
[32] C. Coffman, M. M. Sánchez, F. J. Higuera, and P. C. Lozano, Appl. Phys. Lett. **109**, 231602 (2016).
[33] C. Coffman, Electrically-assisted evaporation of charged fluids: Fundamental modeling and studies on ionic liquids, Ph.D. thesis, Massachusetts Institute of Technology, 2016.
[34] I. G. Loscertales and J. F. de la Mora, J. Chem. Phys. **103**, 5041 (1995).
[35] J. V. Iribarne and B. A. Thomson, J. Chem. Phys. **64**, 2287 (1976).

[36] M. Huang, Y. Jiang, P. Sasisanker, G. W. Driver, and H. Weingartner, J. Chem. Eng. Data **56**, 1494 (2011).
[37] A. Stoppa, O. Zech, W. Kunz, and R. Buchner, J. Chem. Eng. Data **55**, 1768 (2010).
[38] L. G. Sanchez, J. R. Espel, F. Onink, G. W. Meindersma, and A. B. de Haan, J. Chem. Eng. Data **54**, 2803 (2009).
[39] M. E. V. Valkenburg, R. L. Vaughn, M. Williams, and J. S. Wilkes, Thermochim. Acta **425**, 181 (2005).
[40] G. L. R. Mair, Nucl. Instrum. Methods **172**, 567 (1980).
[41] R. Krpoun and H. R. Shea, J. Appl. Phys. **104**, 064511(2008).
[42] C. Schreiner, S. Zugmann, R. Hartl, and H. J. Gores, J. Chem. Eng. Data **55**, 1784 (2010).
[43] Q. S. Liu, J. Liu, X. X. Liu, and S. T. Zhang, J. Chem. Thermodynam. **90**, 39 (2015).
[44] L. D. Landau and E. M. Lifshitz, *Electrodynamics of Continuous Media* (Pergamon Press, London, 1960).
[45] J. R. Melcher, *Continuum Electromechanics* (MIT Press, Cambridge, 1981).
[46] O. A. Basaran and L. E. Scriven, J. Colloid Interface Sci. **140**, 10 (1990).
[47] F. K. Wohlhuter and O. A. Basaran, J. Fluid Mech. **235**, 481 (1992).
[48] C. E. Rosenkilde, Proc. R. Soc. Lond. A **312**, 473 (1969).
[49] M. J. Miksis, Phys. Fluids **24**, 1967 (1981).